

**PREPUBLICACIONES DEL DEPARTAMENTO
DE MATEMÁTICA APLICADA
UNIVERSIDAD COMPLUTENSE DE MADRID
MA-UCM 2012-08**

**Theory of intermittency applied
to classical pathological cases**

Ezequiel del Rio, Sergio Elaskar, and Valeri A. Makarov

Julio-2012

<http://www.mat.ucm.es/deptos/ma>
e-mail:matemática_aplicada@mat.ucm.es

Theory of intermittency applied to classical pathological cases

Ezequiel del Rio^a, Sergio Elaskar^b, and Valeri A. Makarov^c

^a*Departamento de Física Aplicada, ETSI Aeronáuticos, Universidad Politécnica de Madrid, Cardenal Cisneros 3, 28040 Madrid, Spain (e-mail: ezequiel.delrio@upm.es)*

^b*Departamento de Aeronautica. Facultad de Ciencias Exactas, Físicas y Naturales, Universidad Nacional de Córdoba, Avenida Velez Sarfield, 1611, 5000 Córdoba, Argentina (e-mail: ssinha@eng.auburn.edu)*

^c*Dept. of Applied Mathematics, Facultad de Ciencias Matemáticas, Universidad Complutense de Madrid, Av. Complutense s/n, 28040 Madrid, Spain (e-mail: vmakarov@mat.ucm.es)*

Abstract

The classical theory of intermittency assumes uniform density of points reinjected from the chaotic to the laminar region. Though it works fine in some model systems, there exist a number of so-called pathological cases characterized by a significant deviation of main characteristics from the values predicted on the basis of the uniform distribution. Recently we reported on how the reinjection probability density (RPD) can be generalized. Here we extend this methodology and apply it to different dynamical systems exhibiting anomalous Type-II and Type-III intermittencies. We show that one-parametric power law RPD successfully accounts for a variety of significantly different statistics observed in distinct dynamical systems. The obtained RPDs fit well into numerical data and enable analytic estimation of the length of the laminar phase of intermittent behaviors. We also derive and classify characteristic relations between the mean laminar length and main controlling parameter in perfect agreement with the data provided by numerical simulations.

Keywords: Chaos, Intermittency, One dimensional map.

1. Introduction

Intermittency is a particular route to the deterministic chaos characterized by spontaneous transitions between laminar and chaotic dynamics. For the first time this concept has been introduced by Pomeau and Maneville in the context of the Lorenz system [1, 2]. Later the intermittency has been found in a variety of different systems including, for example, periodically forced nonlinear oscillators, Rayleigh-Bénard convection, derivative nonlinear Schrödinger (DNLS) equation, and the development of turbulence in hydrodynamics (see e.g. [3–5]). Proper qualitative characterization of intermittency based on experimental data is especially useful for studying problems with partial or complete lack of knowledge on exact governing equations, as it frequently happens e.g. in Economics, Biology, and Medicine (see e.g. [6, 7]).

The intermittency has been classified in three types called I, II, and III [8]. The local laminar dynamic of Type-I intermittency evolves in a narrow channel, whereas

the laminar behavior of Type-II and Type-III intermittencies develops around a fixed point of generalized Poincare maps:

$$x_{n+1} = (1 + \epsilon)x_n + ax_n^3 \quad \text{Type-II} \quad (1)$$

$$x_{n+1} = -(1 + \epsilon)x_n - ax_n^3 \quad \text{Type-III} \quad (2)$$

where $a > 0$ accounts for the weight of the nonlinear component and ϵ is a controlling parameter ($|\epsilon| \ll 1$). For $\epsilon \gtrsim 0$, the fixed point $x_0 = 0$ becomes unstable, and hence trajectories slowly escape from the origin preserving and reversing orientation for Type-II and Type-III intermittencies, respectively.

Other characteristic attribute of the intermittency is the *global reinjection mechanism* that maps trajectories of the system from the chaotic region back into the *local* laminar phase. This mechanism can be described by the corresponding reinjection probability density (RPD), determined by the chaotic dynamics of the system. Analytical expressions for the RPD are available for a few problems only, hence to describe main statistical properties of intermittency different approximations of the RPD have been employed. The most common approach uses the uniform RPD, which, however, works fine in some model cases only [9–11]. Another approach considers reinjection into a given point in the presence of noise [12–14]. Nevertheless, there exist a number of so-called pathological cases where these approaches fail to explain the behavior of the dynamical systems.

Recently to describe the reinjection mechanism of a wide class of dynamical systems exhibiting intermittency we introduced a generalized RPD, parametric power law function, which includes the uniform reinjection as a particular case [15, 16]. We showed that the shape of the generalized RPD is determined by the behavior of trajectories within chaotic regime in a vicinity of a point in the Poincare map with infinite or zero tangent. Later it has been shown that this mechanism is robust against the external noise [17]. Here we further develop this approach and apply it to pathological cases of intermittency described in the literature [18, 19]. We show that all these cases can be now included in the general theoretical framework.

2. Assessment of RPD function

First let us briefly describe the theoretical framework that accounts for a wide class of dynamical systems exhibiting intermittency. We consider a general 1-D map

$$x_{n+1} = F(x_n), \quad F : \mathbb{R} \rightarrow \mathbb{R} \quad (3)$$

which exhibits intermittency. The RPD function, denoted here by $\phi(x)$, determines the statistical behavior of trajectories and depends on the particular shape of $F(x)$. There is no direct clue on how to derive robustly $\phi(x)$ from experimental or numerical data, specially if only a small data set is available.

Earlier we have shown that the key point to solve this problem is to introduce the following integral characteristics:

$$M(x) = \begin{cases} \frac{\int_{x_s}^x \tau \phi(\tau) d\tau}{\int_{x_s}^x \phi(\tau) d\tau} & \text{if } \int_{x_s}^x \phi(\tau) d\tau \neq 0 \\ 0 & \text{otherwise} \end{cases} \quad (4)$$

where x_s is some “starting” point. Setting a constant $c > 0$ that limits the laminar region we define the domain of M , i.e. $M : [x_0 - c, x_0 + c] \rightarrow \mathbb{R}$, where x_0 is the fixed point of (3) defining the laminar phase of intermittency. In the previous works [15, 16] we used $x_s = x_0$, however, a more general approach sets $x_s = x_0 \pm c$. Below, for the sake of simplicity, we shall assume that $x_s = x_0 - c$.

Since $M(x)$ is an integral characteristics, its numerical estimation is more robust than direct evaluation of $\phi(x)$. This allows reducing statistical fluctuations even for a relatively small data set or data with high level of noise. To approximate numerically $M(x)$, we notice that it is an average over reinjection points in the interval $(x_s, x_0 + c)$, hence we can write

$$M(x) \approx \frac{1}{n} \sum_{j=1}^n x_j, \quad x_{n-1} < x \leq x_n \quad (5)$$

where the data set (reinjection points) $\{x_j\}_{j=1}^N$ has been previously sorted, i.e. $x_j \leq x_{j+1}$.

For a wide class of maps exhibiting Type-II or Type-III intermittency $M(x)$ follows linear law

$$M(x) = \begin{cases} m(x - \hat{x}) + \hat{x} & \text{if } x \geq \hat{x} \\ 0 & \text{otherwise} \end{cases} \quad (6)$$

where $m \in (0, 1)$ is a free parameter and \hat{x} is the lower boundary of reinjections, i.e. $\hat{x} = \inf\{x_j\}$. Then using (4) we obtain the corresponding RPD:

$$\phi(x) = \frac{\alpha + 1}{c^{\alpha+1}} (x - \hat{x})^\alpha, \quad \text{with } \alpha = \frac{2m - 1}{1 - m} \quad (7)$$

For $m = 1/2$ we recover the most common approach with uniform RPD, i.e. $\phi(x) = 1/c$, widely considered in the literature. The RPD (7) has two limit cases:

$$\phi_0(x) = \lim_{m \rightarrow 0} \phi(x) = \delta(x - \hat{x}) \quad (8)$$

$$\phi_1(x) = \lim_{m \rightarrow 1} \phi(x) = \delta(x - c) \quad (9)$$

In the following sections we shall show that the pathological cases of intermittency are close to these limits.

3. Length of laminar phase

Using $\phi(x)$ we can derive the fundamental characteristic of the intermittency, the probability density of the length of the laminar phase. Following [16] we introduce the absolute value of x_n . Then in the laminar phase the dynamics of $|x_n|$ can be approximated by the following differential equation

$$\frac{d|x|}{dl} = \varepsilon|x| + a|x|^3 \quad (10)$$

where l approximates the number of iterations in the laminar region, i.e. the length of the laminar phase. Solving (10) for l we get

$$l(|x|) = \frac{1}{2\varepsilon} \ln \left(\frac{c^2(\varepsilon + a|x|^2)}{x^2(\varepsilon + ac^2)} \right) \quad (11)$$

Since $|x|$ in (11) is a random variable described by $\phi(x)$, the statistics of l is also governed by the global properties of the RPD.

Let $\psi(l)$ be the probability density function of l , then it can be obtained by

$$\psi(l) = 2\phi(X(l)) \left| \frac{dX(l)}{dl} \right| \quad (12)$$

where

$$X(l) = \sqrt{\frac{\varepsilon}{(a + \varepsilon/c^2) e^{2\varepsilon l} - a}} \quad (13)$$

is the inverse function of $l(|x|)$. Thus the pdf of the length of the laminar phase is given by

$$\psi(l) = \phi(X(l)) [aX(l)^3 + \varepsilon X(l)] \quad (14)$$

Using (14) we can determine the mean value of l

$$\bar{l} = \int_0^{\infty} s\psi(s)ds \quad (15)$$

and hence estimate the critical exponent of the characteristic relation $\bar{l} \propto \varepsilon^{-\beta}$ which describes, for small values of ε , how fast the length of the laminar phase grows while ε decreases. The critical exponent β depends on m and \hat{x} according with the following cases:

- Case A: $\hat{x} = x_0$

A1: $m \in (0, 2/3)$. Equations (14) and (15) give

$$\beta = \frac{2 - 3m}{2 - 2m} \quad (16)$$

Particularly $\lim_{m \rightarrow 0} \beta = 1$.

A2: $m \in [2/3, 1)$. Equations (14) and (15) give

$$\beta = 0 \quad (17)$$

- Case B: $\hat{x} > x_0$. There is an upper cut-off for l and in the limit $\varepsilon \rightarrow 0$ the value \bar{l} practically does not change, hence

$$\beta = 0 \quad (18)$$

- Case C: $\hat{x} < x_0$. If $\phi(x_0) \neq 0$ and $\phi'(x_0)$ is bounded, then

$$\beta = \frac{1}{2} \quad (19)$$

as in the uniform reinjection.

In certain situations the described limit values of β can be only reached numerically using prohibitively small values of ε . In particular as we shall show below, in the Case C if $\hat{x} \approx x_0$ the characteristic relation matches the Case A ($\hat{x} = x_0$) for small enough values of ε .

4. Anomalous Type-III intermittency

In this section we apply the theoretical results presented above to the map (3) with

$$F(x) = -((1 + \varepsilon)x + x^3)e^{-dx^2} \quad (20)$$

This dynamical system exhibits Type-III intermittency and the pdf of the laminar length deviates significantly from the prediction made by the classical theory. In Ref. [18] it has been argued that the observed deviation is due to strongly nonuniform reinjection. Let us now show how this reinjection process can be described within our general framework.

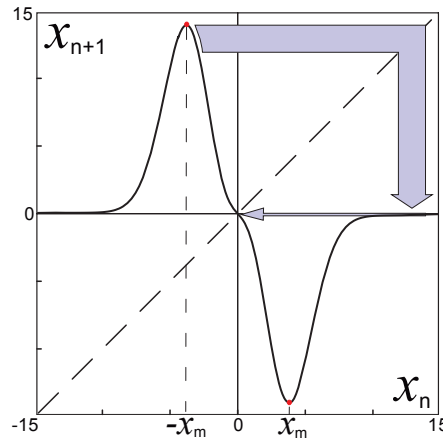


Figure 1: Sketch of the map (3), (20) exhibiting anomalous Type-III intermittency. Thick arrow illustrates mapping of the points from the chaotic region (around the maximum of $F(x)$) into the region with practically zero tangent of $F(x)$ and thin arrow indicates their reinjection to the laminar region.

The map (3), (20) has single unstable ($\varepsilon > 0$) fixed point at $x_0 = 0$. The behavior of trajectories (with direction reversing) near x_0 defines the laminar phase of intermittency. Figure 1 illustrates the reinjection process from the chaotic region around the maximum of $F(x)$ into the laminar region. Note the relative thickness of the arrows reflecting strong compression of the reinjected trajectories, which suggests significantly nonuniform $\phi(x)$. The reinjection point nearest to the origin is given by $\hat{x} = F^2(x_m) \gtrsim 0$. Thus there is a gap around the origin $x \in (-\hat{x}, \hat{x})$ that receives no reinjection. We notice that such reinjection mechanism differs from those proposed in Ref. [16] based on expansion of trajectories around the maximum of $F(x)$. Indeed, here the function $F(x)$ has very small tangent for $|x| \gg 1$, and points around its maximum are mapped into a small region in the laminar zone (Fig. 1).

4.1. Estimation of RPD

To estimate the function M we numerically iterated the map and then evaluated (5). Due to the symmetry of the map, we consider only reinjection points from one side.

As expected the data obtained fit well to the linear law (Fig. 2(a)). Thus we can conclude that the power law (7) generated by trajectories passing around the maximum and minimum of $F(x)$ is robust against strong compression in the reinjection mechanism. Least mean square fit of the data gives $m = 0.0927$ and $\hat{x} = 0.9 \times 10^{-3}$. As expected

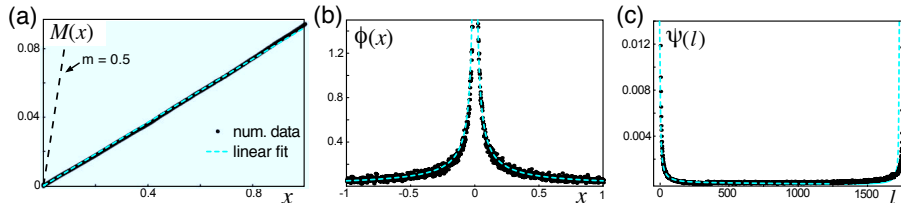


Figure 2: Analysis of the anomalous Type-III intermittency in the map (3), (20) ($d = 0.1$, $\varepsilon = 0.005$, and the laminar interval $[-1, 1]$). a) Assessment of the RPD. Numerical simulation and function $M(x)$ evaluated by (5) (dots). Cyan dashed line corresponds to the least mean square fit. Black dashed line with slope $m = 0.5$ illustrates the function $M(x)$ corresponding to the uniform RPD. b) Numerical RPD. Dashed cyan curve corresponds to (7) with the parameters found in (a). c) Probability density of the length of the laminar phase. Cyan dashed line corresponds to (14).

the slope differs significant from $m = 1/2$ (Fig. 2(a), dashed black line). Substituting the found value into (7) we determine the exponent $\alpha = -0.898$. We note that the analytical value for the lower boundary of reinjections $\hat{x} = F^2(x_m) \approx 10^{-4}$ is close enough to the value found experimentally. In this work we shall use the experimental value \hat{x} instead of the theoretical one to stress the fact that the exact shape of $F(x)$ and the exact value \hat{x} are not necessary to obtain faithful description of all statistic properties of the intermittency.

To crosscheck the obtained results we plotted numerical data and predicted shape of $\phi(x)$ (Fig. 2(b)). Visual inspection confirms good agreement between the numerical data and the analytical expression. We note that for zero-tangent nonlinearity and strong compression of the reinjected trajectories (Fig. 1) the RPD shown in Fig. 2(b) is closed to the limit $\phi_0 = \delta(x - \hat{x})$ as we expected for $m \rightarrow 0$ (see Eq. (8)).

4.2. Length of laminar phase

Earlier two separate analytical arguments to estimate the behavior of $\psi(l)$ in opposite limits ($l \rightarrow 0$ and $l \rightarrow \hat{l}$) have been proposed [18]. We note that our approach provides approximation of $\psi(l)$ in a single shot (see Eq. (14)). Indeed, using the found RPD (Fig. 2(a-b)) we can easily evaluate the pdf for the length of the laminar phase in good agreement with experimental data (Fig. 2(c)).

Since $\hat{x} > x_0 = 0$, according to our classification we are in the Case B and there exists an upper cut-off for l . The cut-off length, \hat{l} , is given by

$$X(\hat{l}) = \hat{x}$$

Hence as $l \rightarrow \hat{l}$ the pdf $\phi(X(l))$ grows to infinity ($\alpha < 0$) and in accordance with (14) $\psi \rightarrow \infty$. It is worth noting that the presence of a cut-off is not a sufficient condition for unbounded growth of ψ as $l \rightarrow \hat{l}$. Besides, it is also necessary that $m \in (0, 1/2)$. In the next section we shall show a counterexample.

The cut-off value \hat{l} increases as ε decreases and in the limit

$$\hat{l}_0 = \lim_{\varepsilon \rightarrow 0} \hat{l}(\varepsilon) = \frac{1}{2a} \left(\frac{1}{\hat{x}^2} - \frac{1}{c^2} \right) \quad (21)$$

which also corresponds to the characteristic exponent $\beta = 0$ [16]. For $d = 0.1$ Eq. (21) gives $\hat{l} \approx 10^{12}$, hence for the values of ε used in Fig. 2(c) we have $\bar{l} \ll \hat{l}$. Since $\hat{x} \approx 0$ the Case A1 ($\hat{x} = 0$) can provide reasonable approximation for the characteristic exponent β . Any decrement of ε must increase the average laminar length \bar{l} up to the asymptotic limit. To confirm this we performed simulations decreasing ε (Fig. 3, circles). Indeed, in a wide range of ε (up to 10^{-7}) the laminar length is governed by the characteristic exponent given by (16).

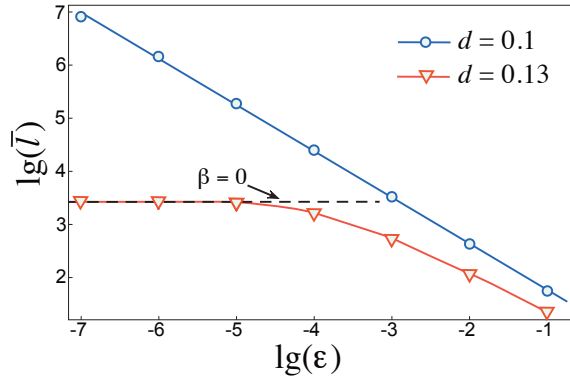


Figure 3: Characteristic relations of the averaged length of the laminar phase \bar{l} vs ε for the map (3), (20). Circles and triangles show numerical data. For $d = 0.1$ the solid line has slope $\beta = 0.885$ in agreement (within 6% of relative error) with the analytical value 0.948 given by (16). For $d = 0.13$ the horizontal dashed line shows the asymptotic behavior of \bar{l} , with $\beta \rightarrow 0$.

However, if we slightly increase the parameter $d = 0.13$, making \hat{x} bigger than before, then the same calculation gives $\hat{l} \approx 10^4$, and hence \bar{l} must rapidly saturate, and then the critical exponent attains the value $\beta = 0$ as expected in the Case B (see Eq. (18)). Our numerical simulations confirms such behavior of \bar{l} (Fig. 3, triangles).

5. Pikovsky intermittency

Another classical example of nonstandard intermittency can be observed in the Pikovsky's map:

$$x_{n+1} = f(x_n) = \begin{cases} G(x_n) & x_n \geq 0 \\ -G(-x_n) & x_n < 0 \end{cases} \quad (22)$$

where $G(x) = x^q + hx - 1$ ($q, h > 0$). The map (22) has no fixed points and to facilitate the study of its dynamics it is convenient to introduce the second iteration, i.e. to consider Eq. (3) with $F(x) = f^2(x) = f(f(x))$. In what follows we shall deal with this new map.

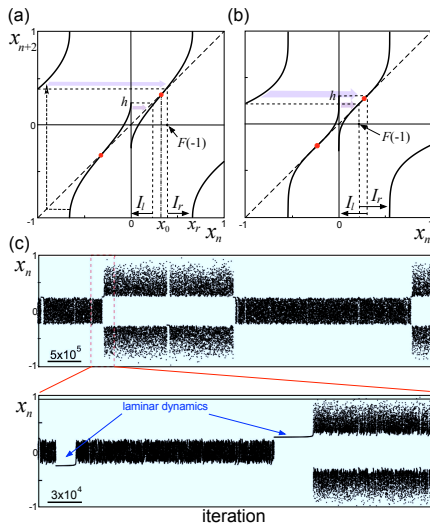


Figure 4: Second iteration of the map (22) demonstrating Type-II (anomalous) intermittency. a) Non-overlapping case with a gap between two reinjection intervals. Arrows show two routs of reinjection into two disjoin intervals I_l and I_r for the upper laminar region. Red dots mark positions of the fixed points. There are two chaotic attractors in the map. b) Slightly overlapping case. Reinjection intervals I_l and I_r overlap. There exists single chaotic attractor. c) Time evolution of the map corresponding to the case (b). Bottom subplot shows zoomed trajectory with two laminar phases near two unstable fixed points ($h = 0.255$, $q = 0.29$).

Figure 4 illustrates the map and an example of a trajectory. Two unstable fixed points (Figs. 4(a) and 4(b), red dots) generate two laminar regions with Type-II intermittency. Since the map is symmetrical, we shall describe the upper fixed point only, i.e. $x_0 > 0$. We define two reinjection intervals $I_l = [h - c, h]$ and $I_r = [F(-1), F(-1) + c]$, where c , as in Sect. 4, is a constant defining extension of the laminar region. Points into the interval I_l are mapped from the branch of $F(x)$ with the end point at $(0, h)$, whereas the interval I_r receives trajectories from the branch starting at $(-1, F(-1))$ (Figs. 4(a) and 4(b), arrows). If $F(-1) > h$ then there is a gap between these intervals (Fig. 4(a)), whereas in the opposite case the intervals overlap (Fig. 4(b)). The trajectory shown in Fig. 4(c) corresponds to the latter case.

In the non-overlapping case there exists two chaotic attractors. Their basins of attraction depend on the controlling parameter q and, by playing with this, we can merge them thus obtaining a single chaotic attractor. In the latter case trajectories can stay for a long time either in the region $|x| < x_0$ or in $|x| > x_0$ and then “jump” between these parts of the attractor (Fig. 4(c), top subplot). The chaotic dynamics is alternated by laminar phases. Figure 4(c), (bottom subplot) shows two laminar phases near the unstable points: one of them just alters the chaotic dynamics in the central part of the attractor, whereas the other leads to transition from the central to the peripheral part of the attractor.

5.1. Non-overlapping case

Let us first assume that $I_l \cap I_r = \emptyset$ (Fig. 4(a)), then the map has two attractors and consequently two independent chaotic behaviors with intermittency selected by the initial condition. Therefore the integral characteristics $M(x)$ has two independent branches.

To evaluate $M(x)$ we set the starting point in (4) to $x_s^r = x_0 - c$ and $x_s^l = x_0 + c$ for the intervals I_r and I_l , respectively. We notice that $\hat{x}_r = \inf_{x_j \in I_r} \{x_j\} \approx F^2(-x_r^+)$, however, $\hat{x}_l = \sup_{x_j \in I_l} \{x_j\} \approx F(0^-)$, thus to adapt the numerical approximation (5) to the interval I_l we sort the reinjection points in reverse order, i.e. $x_j \geq x_{j+1}$.

Figure 5(a) shows two branches of $M(x)$ evaluated over two chaotic attractors. As expected each branch is well approximated by a straight line with $m_l = 0.760$, $\hat{x}_l = 0.252$ and $m_r = 0.723$, $\hat{x}_r = 0.272$ for the interval I_l and I_r , respectively. As in the previous case, we have analytical expressions for $\hat{x}_l = h$ and $\hat{x}_r = h^q + h^2 - 1$, which provide $\hat{x}_l = 0.255$ and $\hat{x}_r = 0.262$, close to the experimental values. Again, as in Sect. 4, we shall use the experimental instead of analytical values to demonstrate that such approximation is good enough to appropriately describe the intermittency.

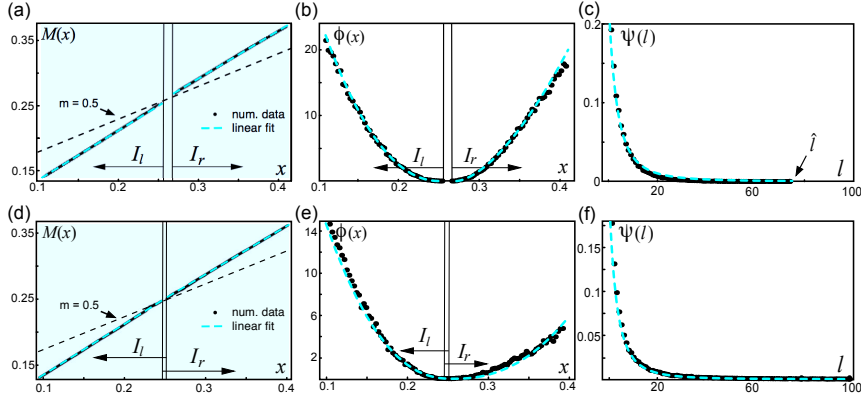


Figure 5: Analysis of the intermittency in the Pikovsky's map in the non-overlapping (top row, $q = 0.29$, $h = 0.255$, two chaotic attractors) and slightly overlapping (bottom row, $q = 0.27$, $h = 0.255$, single chaotic attractor) cases. Results are shown for the second iteration of the map (22). a,d) Numerical data (dots) for two branches of $M(x)$ computed using (5) for reinjections in the intervals I_l and I_r . Dashed cyan lines show the corresponding least mean square fits, which then used to plot $\phi(x)$ and $\psi(l)$. Dashed line with slope $m = 0.5$ corresponds to the uniform RPD. b,e) RPDs for I_l and I_r . Numerical data (dots) and pdfs evaluated by (7) (dashed cyan curves). c,f) Probability density of the length of laminar phase for the interval I_r (for I_l the pdf is similar). Dashed cyan curve corresponds to (14).

For both branches of $M(x)$ the slope is significantly higher than 0.5, which corresponds to infinite tangent generating the power law (7). In Fig. 4(a) this corresponds to the short arrow indicating reinjection into the interval I_l from the region $x \lesssim x_0$ with near infinite tangent of $F(x)$ at $x = 0$. Other singular point is $-x_r$. We notice that points $x \gtrsim -x_r$ are mapped to the region near $F(-1)$ (see dashed trajectory in Fig. 4(a)) and finally, after the second iteration they enter in the laminar interval I_r (long arrow).

Figure 5(b) compares the RPDs evaluated by the power law (7) using the above obtained function $M(x)$ and numerical data. As before (see Fig. 2) the obtained pdf

fits well to the data. Since in this case $(x_0 - \hat{x}_l) > 0$ and $(\hat{x}_r - x_0) > 0$ there is a gap that determines the corresponding cut-off lengths \hat{l}_l and \hat{l}_r . Therefore the length of the laminar phase is bounded. However, in this case we have $m_l, m_r > 0.5$, and hence $\alpha_l, \alpha_r > 0$ and then $\psi(\hat{l}_l) = \psi(\hat{l}_r) = 0$. Thus the asymptotic behavior of the pdf at $l \rightarrow \hat{l}$ is opposite to the blow up observed in Fig. 2(c). Figure 5(c) confirms this conclusion. Note that here, the parameters a and ε used in Eqs. (1) and (14) are given by [19]:

$$a = \frac{1}{6}F'''(x_0), \quad \varepsilon = F'(x_0) - 1 \quad (23)$$

5.2. Slightly overlapping case

In the parameter region $h > F(-1)$ the intervals I_l and I_r overlap and the map has a single chaotic attractor (Figs. 4(b) and 4(c)). The analysis similar to the above described is shown in Figs. 5(d-f).

Here, the mixed RPD is composed of partially overlapping RPDs $\phi_l(x)$ and $\phi_r(x)$ defined on their respective reinjection intervals I_l and I_r . Thus to evaluate the integral characteristics $M(x)$ we separated the numerically obtained reinjection points into two subsets according with their values one iteration before the reinjection into the laminar zone (Fig. 4(b), long and short arrows). Figure 5(d) shows two branches of $M(x)$ evaluated separately over two reinjection subsets. The linear fits give $m_l = 0.770$, $\hat{x}_l = 0.253$ and $m_r = 0.732$, $\hat{x}_r = 0.251$. These values substituted in (7) define $\phi_l(x)$ and $\phi_r(x)$. Finally the composite RPD is given by

$$\phi(x) = \begin{cases} w\phi_l(x) & \text{if } x \leq \hat{x}_r \\ w\phi_l(x) + (1-w)\phi_r(x) & \text{if } \hat{x}_r < x < \hat{x}_l \\ (1-w)\phi_r(x) & \text{if } \hat{x}_l \leq x \end{cases} \quad (24)$$

where w is the statistical weight

$$w = \frac{N_l}{N_r + N_l} \quad (25)$$

where N_l and N_r are the numbers of reinjection points in the intervals I_l and I_r , respectively. The RPD evaluated by (24) is in a good agreement with numerical data (Fig. 5(e)).

The pdf of the laminar length (14) determined by using (24) matches well the numerical data (Fig. 5(f)). We note that the pdfs of the laminar phase of intermittency look similar in the non-overlapping and overlapping cases (Fig. 5(c) vs Fig. 5(f)). In spite of this they differs significantly. In the former case there exists a cut-off length $\hat{l} \approx 75$ and no laminar dynamics with the length above this value can be observed experimentally. In the latter case the probability to find a long enough laminar phase (say, $l \approx 75$) is close to zero but finite.

In the non-overlapping case with the cut-off length (Fig. 5(c)), according to our classification the Case B, we have asymptotically $\beta \rightarrow 0$. On the other hand, in the overlapping region $\phi(x_0) > 0$ and $\phi'(x_0)$ is bounded (Fig. 5(e)), thus we are in the Case C and in the limit $\varepsilon \rightarrow 0$ we get $\beta = 0.5$, which corresponds to the uniform reinjection. As in Sect. 4 we can assume $\hat{x} \approx x_0$ and approximate the critical exponent β following

the limit given in the Case A2, i.e. $\beta \approx 0$. Note, however, that this approximation is worse than we had before because m is close to one. We assume that the overlapped region is very small, consequently $\phi(x_0) \approx 0$, whereas in Sect. 4 $\phi(x_0)$ was unbounded. This means that the set of points reinjected in a small vicinity of x_0 has a low statistical weight and consequently the limit value $\beta = 0.5$ is difficult to reach, i.e. this asymptotic value is observed beyond the numerically accessible parameter region. This situation will be changed if $\phi(x) \neq 0$ as we shall explain in the next subsection.

Figure 6 shows numerical data and theoretical estimation. The blue curve with asymptotic behavior indicated by the straight line labelled by a corresponds to numerical integration of (15) where we used the RPD given by (24). In the region of numerically accessible values of ε this estimate approximates well the numerical data.

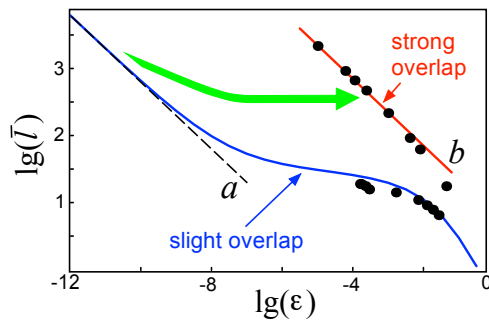


Figure 6: Characteristic relation of the average length of the laminar phase \bar{l} vs ε . Dots correspond to numerical data, whereas blue curve refers to numerical integration of Eq. (15) using (24) as RPD. The asymptotic behavior is given by dashed line (marked by a) with the slope -0.5 ($\beta = 0.5$). The red straight line (marked by b) with the slope -0.5 ($\beta = 0.5$) matches the numerical data for the strongly overlapping case considered in Ref. [19].

5.3. Strongly overlapping case

Until now we studied intermittency in the parameter regions showing either a gap between two RPDs (Fig. 4(a)) or their small overlapping (Fig. 4(b)). In both cases $\phi(x_0)$ is either equal or close to zero. Let us now study the remaining case corresponding to strong overlapping of the intervals I_r and I_l .

Figure 7 shows the RPD obtained for the same parameter set used in Ref. [19] ($h = 0.383$, $q = 0.1$), that corresponds to a strong overlapping of the RPDs $\phi_l(x)$ and $\phi_r(x)$. The RPD has a parabolic shape with high enough $\phi(x)$ in the vicinity of x_0 (fixed point of the map). In this case the overlapped region is bigger than the laminar region, i.e. $(x_0 - c, x_0 + c) \subset (F(-1), h)$, hence from (24) we get the RPD

$$\phi(x) = w\phi_l(x) + (1 - w)\phi_r(x) \quad (26)$$

Since both $F(-1)$ and h lie out of the domain of (5), this approximation cannot provide estimates for \hat{x}_l and \hat{x}_r , instead it gives the limits of the domain of M , i.e. $\hat{x}_l \approx x_0 - c$ and $\hat{x}_r \approx x_0 + c$. We notice, however, that the values m_l and m_r are estimated correctly and hence the RPD (26) accurately describes the numerical pdf (see Fig. 7).

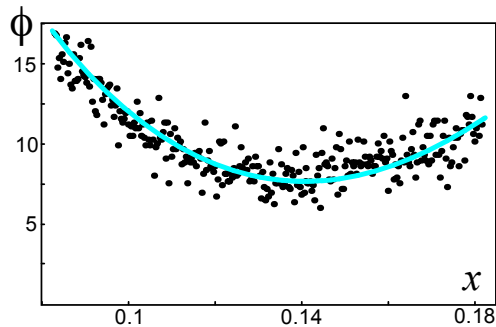


Figure 7: RPD for the Pikovsky's map in the strongly overlapping case. Dots correspond to numerical simulations and the cyan curve is obtained by Eq. (26) with the fitted values for the reinjection on I_l : $m_l = 0.76$ ($\alpha_l = 2.174$). The corresponding values for I_r are $m_r = 0.716$ ($\alpha_r = 1.519$). In this case $N_l/N_r = 0.86$.

Contrary to the case of slight overlapping discussed above now we have $\phi(x_0) \neq 0$ (Fig. 7). Thus we are in the Case C of our classification of the characteristic relation (see Sect. 3), hence we recover $\beta = 0.5$ even for large enough values of ε (up to $\varepsilon \approx 0.5$). Consequently all statistics are compatible with the uniform reinjection, despite of the fact that the obtained RPD is non-uniform (Fig. 7). Figure 6 (strong overlap) shows the characteristic relation between \bar{l} and ε for this case. The green arrow represents the continuous transition of the characteristic relation as the overlapped region increases from very small (blue curve) to large values (red line).

6. Conclusions

Pathological cases of intermittency described in the literature are known by their significant deviation of the main characteristics (e.g. the length of the laminar phase) from those predicted by the classical theory. In this work we have shown that the use of generalized Reinjection Probability Density provides faithful description of anomalous and standard intermittencies in the unified framework. The generalized RPD taken in the form of a power-law function can be fitted to the experimental or numerical data. Moreover the proposed procedure can cope with relatively reduced data sets, which makes it useful for experimental applications. We demonstrated the method on two particular but canonical cases of the Type-II and Type-III intermittencies.

Calculation of the RPD is based on the earlier introduced integral characteristic $M(x)$, which is a linear function with slope $m \in (0, 1)$ that determines the type of RPD. In particular, $m = 0.5$ corresponds to the classical uniform RPD, whereas the limit cases ($m \approx 0$ and $m \approx 1$) describe the anomalous intermittency. For anomalous Type-III intermittency we have found the lowest value of $m \approx 0.09$ observed up to now. This value predicts the RPD close to delta function centered at zero, i.e. $\phi_0(x) = \delta(x)$. The second anomalous case, the Pikovski intermittency (second iteration of the Pikovski's map), corresponds to the Type-II intermittency and high values of m . We got $m \approx 0.77$, which is the biggest value found up to now. In this case the RPD is close to $\phi_1(x) = \delta(x-c)$ and consequently $\phi(x) \gtrsim 0$ in the vicinity of small values of x , which is opposite to Type-III case.

We have shown that the obtained RPDs are in a good agreement with numerical data, and hence our approach is robust against strong length compression. The Type-III intermittency exhibits atypical density of the laminar length, l , which has been accurately described by the approach.

For the Pikovski intermittency we described two different cases of the anomalous statistics with similar values of m . One of them corresponds to the existence in the phase space of two chaotic attractors, whereas the other has single attractor. In the map these cases differ by overlapping of reinjection intervals (non-overlapping vs slightly overlapping). The existence of two reinjection intervals provides two reinjection mechanisms and two RPDs defined over each interval. Thus to obtain them we separated all reinjection points into two independent sets according with their origin just before the reinjection. Finally, the RPDs evaluated over each data set provide the composite RPD describing the dynamics of the system. We have shown that the obtained RPD and the corresponding probability density of the length of the laminar phase are in good agreement with numerical simulations.

We have also introduced classification of different cases of intermittency showing different critical exponents ($\bar{l} \propto \varepsilon^{-\beta}$) based on the parameters of $M(x)$. According to this classification the Type-III intermittency, depending on the parameters, can have two characteristic exponents for the numerically accessible values of the controlling parameter. Since there is a cut-off length \hat{l} even in the limit $\varepsilon \rightarrow 0$, we get $\beta = 0$ in the parameter region $\log(\bar{l}) \lesssim \log(\hat{l}_0)$. However, if $\log(\bar{l}) \ll \log(\hat{l}_0)$ then assuming $\hat{x} \approx 0$ we obtained $\beta = (2 - 3m)/(2 - 2m)$, in good agreement with numerical data ($\beta \approx 0.9$). We note that both cases are far from the classical value $\beta = 0.5$. For the Pikovski intermittency the characteristic exponent depends on the level of overlapping of two reinjection intervals. In the non-overlapping case we have $\beta = 0$. For slight overlapping and $\hat{x}_r < x_0$ this exponent should be $\beta = 0.5$, but it happens in the parameter region for which $\phi(x) \approx 0$ in the vicinity of x_0 (since $m > 2/3$). Such limit is difficult to be reached due to very low number of reinjected points there. Finally for strong overlapping we recover the limit $\beta = 0.5$ predicted by the classical theory assuming the uniform RPD, in spite of the non-uniform RPD in this case.

7. Acknowledgements

This work has been supported by the Spanish Ministry of Science and Innovation under Project FIS2010-20054, by the CONICET under Project PIP 11220090100809, and by grants of the National University of Córdoba and MCyT of Argentina.

- [1] P. Manneville and Y. Pomeau, Phys. Lett. A **75**, 1-2 (1979).
- [2] Y. Pomeau and P. Manneville, Comm. in Math. Phys. **74**, 189-197 (1980).
- [3] M. Dubois, M. Rubio and P. Berge, Phys. Rev. Lett. **51**, 1446-1449 (1983).
- [4] E. del Rio, M.G. Velarde and A. Rodríguez-Lozano, Chaos, Solitons and Fractals **4**, 2169-2179 (1994).
- [5] S.G. Stavrinides, A.N. Miliou, Th. Laopoulos, A.N. Anagnostopoulos, Int. J. Bifurc. Chaos **18**, 1561-1566 (2008).

- [6] J. Zebrowski and R. Baranowski, *Physica A* **336**, 74-83 (2004).
- [7] A. Chian, *Lecture Notes in Economics and Mathematical Systems* Vol. 592, *Complex Systems Approach to Economic Dynamics*, (2007) pp. 39-50. Springer Berlin Heidelberg.
- [8] H. Schuster and W. Just, "Deterministic Chaos. An Introduction", WILEY-VCH Verlag GmbH & Co. KGaA, Weinheim, Germany (2005).
- [9] P. Manneville, *Le Journal de Physique* **41**, 1235-1243 (1980).
- [10] C.M. Kim, O.J. Kwon, E.K. Lee, and H. Lee, *Phys. Rev. Lett.* **73**, 525-528 (1994).
- [11] J.H. Cho, M.S. Ko, Y.J. Park, and C.M. Kim, *Phys. Rev. E* **65**, 036222 (2002).
- [12] C.M. Kim, G.S. Yim, J.W. Ryu and Y.J. Park *Phys. Rev. Lett.* **80**, 5317-5320 (1998).
- [13] W.H. Kye and C.M. Kim, *Phys. Rev. E* **62**, 6304-6307 (2000).
- [14] A.A. Koronovskii and A.E. Hramov, *Eur. Phys. J. B* **62**, 447-452 (2008).
- [15] E. del Rio and S. Elaskar, *Int. J. of Bifurc. Chaos* **20**, 1185-1191 (2010).
- [16] S. Elaskar, E. del Rio, and J. M. Donoso, *Physica A* **390**, 2759-2768 (2011).
- [17] E. del Rio, M.A.F. Sanjuán, and S. Elaskar, *Commun. Nonlinear Sci. Numer. Simulat.* **17**, 3587-3596 (2012).
- [18] J. Laugesen, N. Carlsson, E. Mosekilde and Bountis, *Open System & Information Dynamics* **4**, 393-405 (1997).
- [19] A.S. Pikovsky, *J. Phys A* **16**, L109-L112 (1983).

**PREPUBLICACIONES DEL DEPARTAMENTO
DE MATEMÁTICA APLICADA**
UNIVERSIDAD COMPLUTENSE DE MADRID
MA-UCM 2011

1. APPROXIMATING TRAVELLING WAVES BY EQUILIBRIA OF NON LOCAL EQUATIONS, J. M. Arrieta, M. López-Fernández and E. Zuazua.
2. INFINITELY MANY STABILITY SWITCHES IN A PROBLEM WITH SUBLINEAR OSCILLATORY BOUNDARY CONDITIONS, A. Castro and R. Pardo
3. THIN DOMAINS WITH EXTREMELY HIGH OSCILLATORY BOUNDARIES, J. M. Arrieta and M. C. Pereira
4. FROM NEWTON EQUATION TO FRACTIONAL DIFFUSION AND WAVE EQUATIONS, L. Vázquez
5. EL CÁLCULO FRACCIONARIO COMO INSTRUMENTO DE MODELIZACIÓN, L. Vázquez and M. P. Velasco
6. THE TANGENTIAL VARIATION OF A LOCALIZED FLUX-TYPE EIGENVALUE PROBLEM, R. Pardo, A. L. Pereira and J. C. Sabina de Lis
7. IDENTIFICATION OF A HEAT TRANSFER COEFFICIENT DEPENDING ON PRESSURE AND TEMPERATURE, A. Fraguera, J. A. Infante, Á. M. Ramos and J. M. Rey
8. A NOTE ON THE LIOUVILLE METHOD APPLIED TO ELLIPTIC EVENTUALLY DEGENERATE FULLY NONLINEAR EQUATIONS GOVERNED BY THE PUCCI OPERATORS AND THE KELLER–OSSERMAN CONDITION, G. Díaz
9. RESONANT SOLUTIONS AND TURNING POINTS IN AN ELLIPTIC PROBLEM WITH OSCILLATORY BOUNDARY CONDITIONS, A. Castro and R. Pardo
10. BE-FAST: A SPATIAL MODEL FOR STUDYING CLASSICAL SWINE FEVER VIRUS SPREAD BETWEEN AND WITHIN FARMS. DESCRIPTION AND VALIDATION. B. Ivorra B. Martínez-López, A. M. Ramos and J.M. Sánchez-Vizcaíno.
11. FRACTIONAL HEAT EQUATION AND THE SECOND LAW OF THERMODYNAMICS, L. Vázquez, J. J. Trujillo and M. P. Velasco
12. LINEAR AND SEMILINEAR HIGHER ORDER PARABOLIC EQUATIONS IN \mathbb{R}^N , J. Cholewa and A. Rodríguez Bernal
13. DISSIPATIVE MECHANISM OF A SEMILINEAR HIGHER ORDER PARABOLIC EQUATION IN \mathbb{R}^N , J. Cholewa and A. Rodríguez Bernal
14. DYNAMIC BOUNDARY CONDITIONS AS A SINGULAR LIMIT OF PARABOLIC PROBLEMS WITH TERMS CONCENTRATING AT THE BOUNDARY, A. Jiménez-Casas and A. Rodríguez Bernal
15. DISEÑO DE UN MODELO ECONÓMICO Y DE PLANES DE CONTROL PARA UNA EPIDEMIA DE PESTE PORCINA CLÁSICA, E. Fernández Carrión, B. Ivorra, A. M. Ramos, B. Martínez-López, Sánchez-Vizcaíno.
16. BIOREACTOR SHAPE OPTIMIZATION. MODELING, SIMULATION, AND SHAPE OPTIMIZATION OF A SIMPLE BIOREACTOR FOR WATER TREATMENT, J. M. Bello Rivas, B. Ivorra, A. M. Ramos, J. Harmand and A. Rapaport

17. THE PROBABILISTIC BROSAMLER FORMULA FOR SOME NONLINEAR NEUMANN BOUNDARY VALUE PROBLEMS GOVERNED BY ELLIPTIC POSSIBLY DEGENERATE OPERATORS, G. Díaz

**PREPUBLICACIONES DEL DEPARTAMENTO
DE MATEMÁTICA APLICADA**
UNIVERSIDAD COMPLUTENSE DE MADRID
MA-UCM 2012

1. ON THE CAHN-HILLIARD EQUATION IN $H^1(\mathbb{R}^N)$, J. Cholewa and A. Rodríguez Bernal
2. GENERALIZED ENTHALPY MODEL OF A HIGH PRESSURE SHIFT FREEZING PROCESS, N. A. S. Smith, S. S. L. Peppin and A. M. Ramos
3. 2D AND 3D MODELING AND OPTIMIZATION FOR THE DESIGN OF A FAST HYDRODYNAMIC FOCUSING MICROFLUIDIC MIXER, B. Ivorra, J. L. Redondo, J. G. Santiago, P.M. Ortigosa and A. M. Ramos
4. SMOOTHING AND PERTURBATION FOR SOME FOURTH ORDER LINEAR PARABOLIC EQUATIONS IN \mathbb{R}^N , C. Quesada and A. Rodríguez-Bernal
5. NONLINEAR BALANCE AND ASYMPTOTIC BEHAVIOR OF SUPERCRITICAL REACTION-DIFFUSION EQUATIONS WITH NONLINEAR BOUNDARY CONDITIONS, A. Rodríguez-Bernal and A. Vidal-López
6. NAVIGATION IN TIME-EVOLVING ENVIRONMENTS BASED ON COMPACT INTERNAL REPRESENTATION: EXPERIMENTAL MODEL, J. A. Villacorta-Atienza and V.A. Makarov
7. ARBITRAGE CONDITIONS WITH NO SHORT SELLING, G. E. Oleaga
8. THEORY OF INTERMITTENCY APPLIED TO CLASSICAL PATHOLOGICAL CASES, E. del Rio, S. Elaskar, and V. A. Makarov